Results in Surfaces and Interfaces 20 (2025) 100625

Contents lists available at ScienceDirect

Results in Surfaces and Interfaces

journal homepage: www.elsevier.com/locate/rsurfi

Surface modification of aluminum on a silicon chip by citric acid treatment

Moataz Mekawy [a], Kazuya Iida [a], Akitsu Shigetou [b], Jin Kawakita [a,*]

[a] Research Center for Macromolecules and Biomaterials, National Institute for Materials Science, 1-1 Namiki, Tsukuba, Japan
[b] Research Center for Materials Nanoarchitectonics (MANA), National Institute for Materials Science, 1-1 Namiki, Tsukuba, Japan

ARTICLE INFO

Keywords:
Aluminum
Surface treatment
Citric acid
Sensor
Moisture

ABSTRACT

Aluminum is widely used as a conductive material in the semiconductor and electronics fields. However, the inevitable formation of an oxide layer on its surface during atmospheric heat treatment accompanying the fabrication process increases surface resistivity. This necessitates a surface treatment to mitigate the negative effects of the oxide layer. In this study, a silicon chip containing aluminum wires was immersed in a 0.1 wt% citric acid solution as a simple surface treatment technique. In situ electrical current measurements from arrays of aluminum wires located on the silicon chip were performed during the treatment. X-ray photoelectron spectroscopy and infrared spectroscopy were conducted before and after the treatment. The results revealed a significant removal of the contamination/oxide layer formed on the chip surface, and the outermost stacked layer on the aluminum surface turned hydrophilic (ca. 0.3 Å/min at 50 °C), resulting in a considerable decrease in the electric resistance around the surface. As a demonstration, a sensor made of Al and Au arrays was placed on the silicon chip, and the citric acid treatment helped enhance its response to humid air by more than 1000, with the steady current response realized in a treatment time of 2–3 min. This promising surface treatment method is expected to help enhance the removal of oxide layers formed on metal-based components.

1. Introduction

Aluminum is widely used as a conductive material for electric wirings in the semiconductor and electronic fields. During the fabrication process of semiconductor chips and integrated circuit boards, an oxide layer is inevitably formed on the aluminum surface in air. This oxide layer spontaneously grows during heat treatment processes, such as solder reflow and resin molding, which are generally conducted in the mounting or packaging steps [1]. The thickness of the aluminum oxide layer (AOL) formed mainly depends on the time and temperature of the heat treatment processes [2,3]. The AOL layer is responsible for the surface passivation or corrosion of aluminum [4]. Conducting the heat treatment in vacuum may help suppress the growth of the AOL on the aluminum metal surface, given the absence of any vapor source or oxidizing gas. However, this incurs additional costs, particularly for the mass production of semiconductor processing technologies. Therefore, an appropriate surface treatment to adequately remove or suppress the AOL while preserving the excellent surface reactivity of aluminum is warranted.

A small amount of condensed liquid water or aggregated adsorbed water molecules can be successfully detected using arrays of Al and Au metals (micro width) arranged with interdigitated displacements with sub-micron gaps on a silicon chip covered with an insulating silica layer. A galvanic current flows between the Al and Au arrays when the liquid and aggregated adsorbed molecules of water contact along the adjacent lines to form a bridge, and the current is then measured [5,6]. This principle can help detect the early stages of dew condensation and measure small amounts of transpiration of plants and evaporation of sweat; thus, it has promoted the development of chips, packages, and electric circuits for sensor applications. The metal lines on the sensor chip are exposed to air during the fabrication process, particularly during heat treatment processes, such as solder reflow and the mounting process for the mold package and electronic circuit board [7]. The AOL is easily formed on the aluminum metal line, leading to an increase in the electrical resistance between the Al and Au lines, that is, the decrease in the galvanic current corresponds to the sensitivity of the sensor application. Therefore, the removal of the AOL on the aluminum surface as well as the suppression of its growth during the fabrication and mounting processes of the chip, is paramount to ensuring the quality of the fabricated chips.

To date, numerous methods have been reported for AOL removal [8]: 1) Mechanical methods employing polishing, scraping, or brushing.

* Corresponding author.
E-mail address: KAWAKITA.Jin@nims.go.jp (J. Kawakita).

https://doi.org/10.1016/j.rsurfi.2025.100625
Received 16 December 2024; Received in revised form 14 August 2025; Accepted 15 August 2025
Available online 16 August 2025
2666-8459/© 2025 The Authors. Published by Elsevier B.V. This is an open access article under the CC BY-NC license (http://creativecommons.org/licenses/by-nc/4.0/).

These methods, however, are ineffective in removing oxide layers formed on curved or rough surfaces. 2) Laser-controlled methods, which can effectively remove the AOL from mainly flat surfaces while reducing substrate damage and environmental contamination [9]. These methods require additional safety measures and are uneconomical. Furthermore, they cannot provide effective AOL removal from finely textured structures, such as our developed chip, as mentioned above. 3) Acid treatment methods employing ammonium bifluoride, phosphoric acid, citric acid and aluminum chloride/ionic liquid [10–12]. These methods are preferable in terms of environmental and substrate protection and are expected to work effectively to reduce the AOL in designed structures.

Citric acid (CA, chemical formula: $C_6H_8O_7$), which is a natural organic polycarboxylic acid, is a representative cost-effective candidate that has been used in acid treatment methods 3), given its nontoxicity and presence of three reactive carboxyl groups [13]. Some researchers have demonstrated its effective use as a cross-linker agent [14–17], a disinfectant and an environmental remediation precursor [18], and a sterilizing agent [19,20]. Another study demonstrated the interaction between CA and the formed AOL. An aqueous solution of CA formed a complex with the AOL. This complex was easily rinsed with some amount of water. Thus, the recovered surface of the Al electrode was obtained [21,22]. The effect of CA concentration was previously examined, and 0.1 wt% of CA can be considered the effective concentration for AOL removal. Higher concentrations may lead not only to the complete removal of AOL but also to the dissolution of aluminum metal [23]. However, the reaction mechanism of the AOL with CA remains unclear, particularly from compositional and kinetic standpoints related to the changes in the surface structure of aluminum.

The objective of this study was to examine the effect of 0.1 wt% CA solution on the oxide layer formed in Al lines in a fabricated chip. For this purpose, the temporal change in the galvanic current measured from the chip was evaluated from a kinetic standpoint during the treatment process with the CA solution at different temperatures. In addition, the surface state of the chip containing Al upon CA treatment was characterized using microscopic observations and spectroscopic analyses from a compositional standpoint. Moreover, the current response at a set humidity for sensor application was compared among the tested chips treated by CA at various temperatures and accumulation times to optimize the treatment conditions for the aluminum lines on the chip.

2. Experimental procedure

2.1. Preparation of test chip and measurement of current from chip

The fabrication of the test chip used in this study has been described in detail elsewhere. Briefly, a wiring process was used to prepare line patterns of Al and Au metals, mainly through the repetition of organic resist coating, photolithography, metal deposition, and lift-off [24]. All the materials used for the chip were of semiconductor fabrication grade. In this study, the lines of Al and Au were 150 each in number and 2.0 and 0.2 μm in width and height, respectively, and 0.5 μm in space between the adjacent lines. Packaging of the chip has also been described in detail elsewhere. Briefly, the chip was placed on an Al lead frame, followed by wire bonding and resin molding at a temperature of 175 °C for 120 s in air [7]. The galvanic current between the Al and Au lines on the chip was measured using an electronic circuit board, as shown in Fig. 1, to amplify the analog signal from the chip and output it in both analog and digital formats to external data processing instruments, such as a PC and data logger. The chips and the electronic circuit boards used in this study were fabricated by Aquze Co., Ltd.

2.2. Surface treatment of chip with citric acid

Fig. 2 shows a schematic of the experimental setup used for the surface treatment of the test chip with the citric acid (CA) solution, as illustrated by the cross-section of the electronic circuit board equipped with the chip, as shown in Fig. 1. Twenty microliters of 0.1 wt% CA aqueous solution was prepared using CA (Kanto Chemical Co., Inc., min. 99.0 % in purity) and ultrapure water (Merck Millipore Corporation, Direct-Q UV3) and dropped onto the chip surface, whereas the CA solution was contained in the frame of the mold resin surrounding the chip. The temperature of the chip surface was controlled using a temperature-controlling instrument (model: CPS-30; AS ONE CORPORATION) by thermal conduction through the components of the experimental setup, as illustrated in Fig. 2. The temperature of the test chip was calibrated in advance using previous techniques [7] and set to 25, 50 and 75 °C in this study. The electric current from the chip was measured for up to 20 min at intervals of 1 s using an electronic circuit board composed of an amplifier and an A/D converter, as shown in Fig. 2. Electrical measurements were performed thrice at the set temperature. Finally, the test chip was thoroughly rinsed with ultrapure water and dried under nitrogen gas flow. Specifications and suppliers of the experimental materials are listed in Table 1.

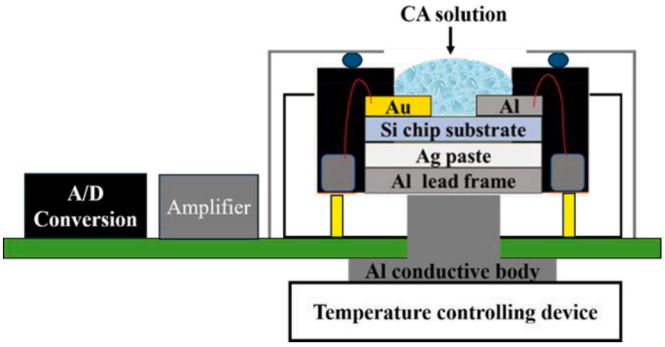

Fig. 2. Schematic of the experimental setup used for the surface treatment of the test chip with citric acid (CA) solution under temperature control and measurement of the current from chip.

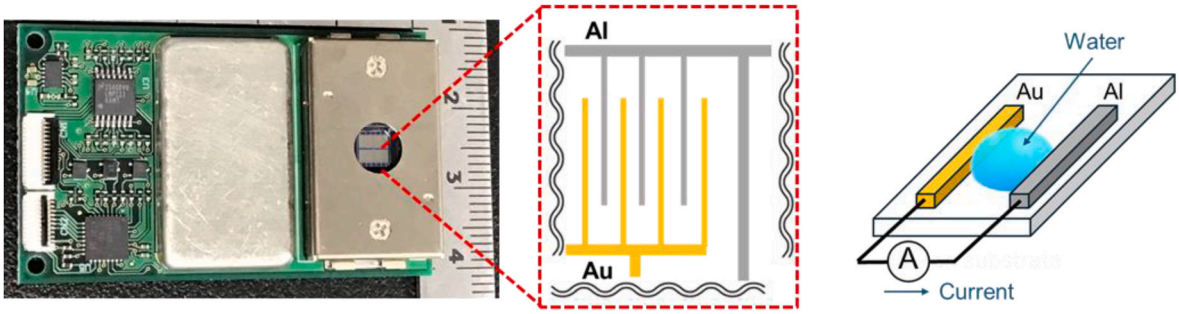

Fig. 1. Image of an electronic circuit board equipped with a chip for electric current measurement, on which lines of Al and Au are arranged like interdigit, as drawn schematically; electric current flows between the Au and Al lines in contact with water.

Table 1
Material specifications and suppliers.

Item	Specification	Supplier
Test chip	Semiconductor fabrication grade	Aquze Co., Ltd
Electronic circuit board	Current range: 10^{-12}~2.5 × 10^{-8} A	Aquze Co., Ltd
Citric acid	Purity: >99.0 %	Kanto Chemical Co., Inc.
Ultra-pure water	Resistivity: >18.2 MΩ cm	Merck Millipore Corporation

2.3. Characterization of chip surface

The surfaces of the test chips were examined under an optical microscope (KEYENCE, VHX 7000 series) and a field-emission scanning electron microscope (SEM; Hitachi Co. Ltd., TM4000). The chemical binding state of the chip surface was examined using X-ray photoelectron spectroscopy (XPS; ULVAC ESCA1600). XPS observations were performed thrice (with Mg–Ka source; 1253.6 eV and 400 W) for each spectrum, and the average was taken. For the overall composition analysis (hereinafter wide scan), a pass energy of 117.4 eV, a dwell time of 5.0 × 10^{-2} s, and an analysis step of 1.0 eV were used. For the curve fitting analysis (hereinafter narrow scan), the spectra were acquired with a pass energy of 23.5 eV, a dwell time of 1.0 × 10^{-2} s, and an analysis step of 0.1 eV. The pass energy and dwell time were machine-dependent. After the narrow scans were performed, the narrow scan spectra were processed using the ULVAC-PHI MultiPak software for curve fitting to extract the differences in the chemical binding state. Curve fitting was automatically performed using the Gaussian least-squares method. Given the anticipated presence of a thin layer composed of metal, reduced native metal oxide, and metal carboxylate on the Al surface following the CA treatment, the Gaussian fitting method was selected as one of the most averaged and applicable fitting methods for various elements. However, because the top surface layer is thin, some elements may have noisy peaks, and the Gaussian fitting method inevitably results in a considerable error in the peak tail regions, a fitting percentage of 80 % or higher was considered acceptable in this study. In addition to the normal scanning mode, an angle-resolved mode with different detection angles was used. Attenuated total internal reflectance Fourier-transform infrared spectroscopy (ATR-FTIR; SHIMADZU Corporation, AIM9000) of the chip surface was performed to identify the chemical structure of the composite generated on the surface.

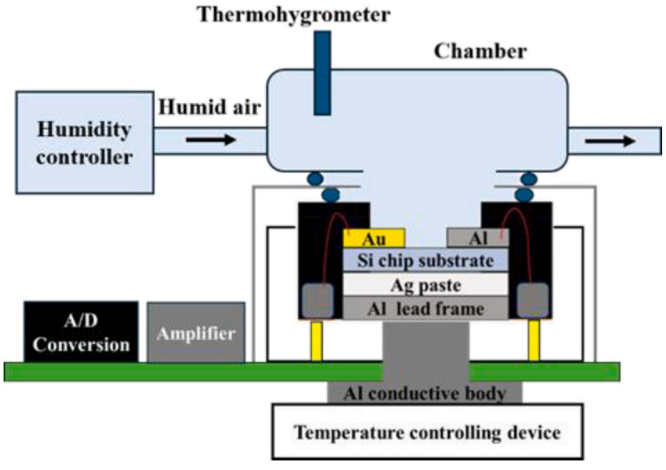

Fig. 3. Schematic of the setup used for the measurement of the sensor response with the test chip to humid air.

2.4. Measurement of sensor response to humid air

Fig. 3 illustrates the experimental setup used to measure the sensor response under controlled relative humidity. The chip surface was exposed inside the chamber, and the temperature of the sensor surface was controlled at 20 °C using the technique described in Section 2.2. After the introduction of compressed air with a relative humidity of approximately 15 % at 25 °C to the chamber for 10 min at a flow rate of 200 normal cubic centimeters per min (NCCM), the set relative humidity on the sensor surface was adjusted to 80 %, 90 %, 100 %, and 110 %, and maintained for 15 min by controlling the vapor pressure inside the chamber using a precision humidity controller (micro equipment Inc., me-40DP-H60MFC-2 PL-FH-OS). The temperature and relative humidity inside the chamber were measured using a thermohygrometer (E + E Elektronik, EE23). In this study, the set relative humidity of 110 % was the nominal value, indicating that the excess of the vapor pressure over the saturated pressure calculated on the sensor surface was condensed. The electric current from the chip was measured at intervals of 1 s using an electronic circuit board composed of an amplifier and an A/D converter, which was explained in section 2.1.

3. Results and discussion

3.1. Changes in the chemical structure of aluminum surface by citric acid solution treatment

Fig. 4 shows the Al2p and O1s XPS spectra of the chip surface before and after treatment with a 0.1 wt% citric acid (CA) solution for 10 min. The detection angle was set to 30° to study the changes in the chemical binding state of the outermost surface. Al2p and O1s were studied to confirm adequate removal of the initial contamination, improvement in the electrical conductivity owing to the partial removal of the natural oxide film by CA cleaning, and improvement in water vapor adsorption owing to the formation of a hydrophilic surface layer. The peak-fitting results were superimposed onto the observed spectra. The chemical binding conditions before and after the CA treatment are denoted by Pristine and CA, respectively.

The chemical binding states of Pristine and CA exhibited notable differences, as evidenced by the binding energy and intensity of the deconvoluted peaks in Al2p shown in Fig. 4(a) and (b). For the pristine sample (Fig. 4(a)), the spectrum showed three peaks. Assuming that the surface of the Al wires was covered with porous native oxide and thick hydrated Al-oxide (AlO_x–H_2O) [25] because of hydrocarbon contamination from the wet etching patterning process and sample transfer in normal air, the deconvoluted peak with the highest intensity was assigned to AlO_x–H_2O. The binding state of the other peaks was defined using the energy gaps (i.e., the difference in the chemical binding structure) from the AlO_x–H_2O peak, according to the XPS database [26]. This is because the binding energy values often shift easily, even on the same surface, due to local differences in the chemical and physical structures. In Fig. 4(a), the energy gaps from AlO_x–H_2O were set to −1.6 eV and −2.8 eV for AlO_x and Al, respectively. In contrast, for the CA sample (Fig. 4(b)), the $Al(OH)_x$ peak clearly appeared, and the Al peak intensified, indicating a CA-based reduction of the native oxide and the formation of a new surface layer. Assuming that the initial organic contaminants were removed by CA and that a thin surface layer containing Al carboxylate and hydroxide was formed on the surface of the partially reduced native oxide, the major component at the XPS detection depth was considered to be AlO_x. Therefore, the deconvoluted peak with the maximum intensity was assigned to AlO_x [27], and the other peaks were identified using the peak gaps from AlO_x. In Fig. 4(b), the energy gaps from AlO_x were set to +1.7 eV [28] and −1.2 eV [29] for Al $(OH)_x$ and Al, respectively. The values of these peak gaps were derived from previous studies on Al oxides and Al subjected to similar acid surface treatments. O1s in Fig. 4(d) is the final state of oxygen bonding in the entire sample, including Si–O, and detailed peak identification is

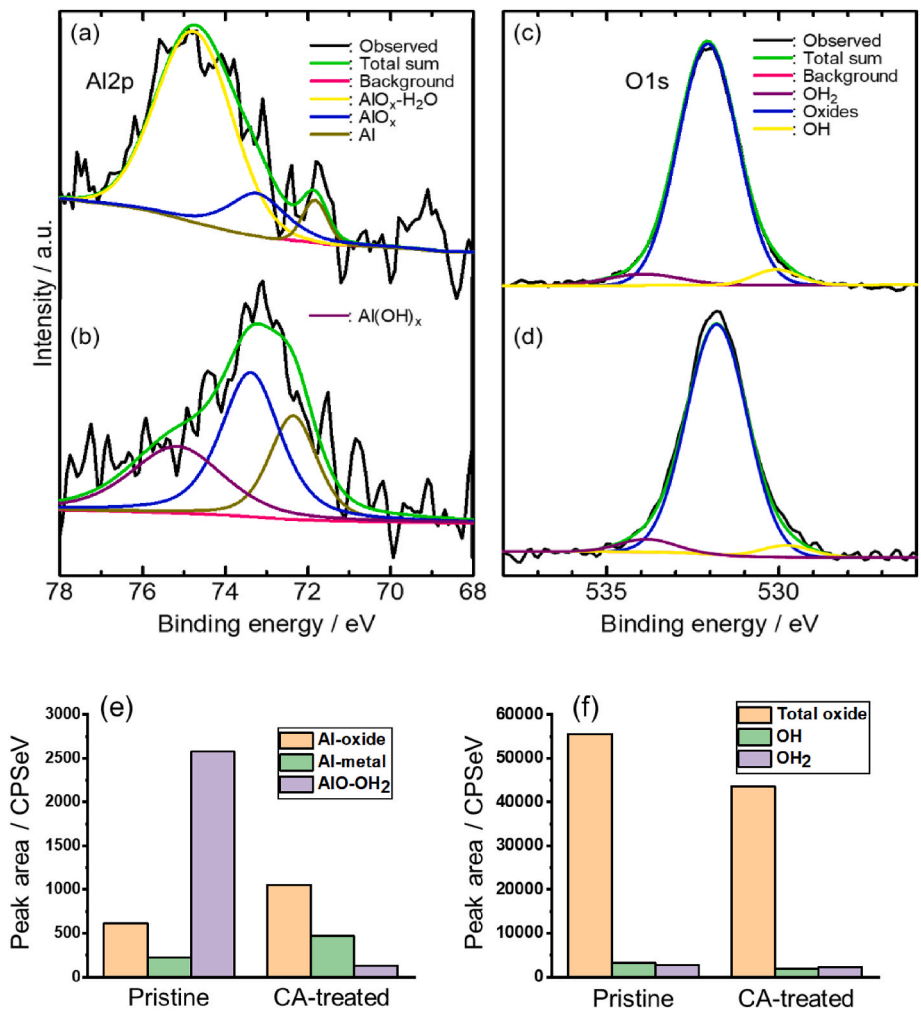

Fig. 4. XPS spectra for Al2p (a, b) and O1s (c, d) of the chip surface before (a, c) and after (b, d) treatment with 0.1 wt% CA solution for 10 min at a temperature of 50 °C and an incident angle of 30°. The peak areas are calculated from Al2p (e) and O1s (f). Background subtraction is done using Shirley equation.

difficult; however, the hydroxyl group that contributes to hydrophilicity is clearly present. These differences in the chemical binding state are summarized based on the atomic concentration, which is denoted by the peak area of each deconvoluted peak, as shown in Fig. 4(e) and (f). The atomic concentration of Al clearly increased for Al2p in the CA sample. This indicates that the thickness of the initial thick surface layer, including the native oxide film, decreased, which is consistent with the tendency for dielectric breakdown and electrical conduction to be easily acquired after the CA treatment. In addition, it is considered that Al $(OH)_x$ originating from the thin surface layer formed by the CA treatment and the subsequent sample transfer, that is, OH in the solution and atmospheric exposure, are possible reasons for this hydration.

Furthermore, the layered structure was confirmed using the angle-resolved technique. Equation (1) can be used to calculate the thickness of the layer, including each chemical binding structure, given the spectra obtained at a detection angle of 45°, which are curve-fitted with the same peak gap values of 30°.The calculation was performed using Al2p spectra[30].

$$I_{30} / I_{45} = exp(-\mathrm{x} / \lambda \sin\Delta\theta) \quad (1)$$

Here, x is the layer thickness, I_{30} and I_{45} are the peak areas derived from the spectra obtained at detection angles of 30° and 45°, respectively, λ is the inelastic mean free path (IMFP) of the surface layer material. In this calculation, the IMFP value of 25.15 Å was used for Al-oxide [31], and the same value was applied to Al-OH_2 for simplicity, because the IMFP of Al-OH_2 is difficult to measure directly. $\Delta\theta$ is the difference between the angles of measurements (15°). Equation (1) can be rearranged to estimate the thickness of the layer before and after the surface treatment using Equation (2).

$$x = -\lambda(\sin\Delta\theta)[\ln (I_{30} / I_{45})] \quad (2)$$

Table 2 presents the calculated results. The calculations show that the thickness of the Al-oxide layer decreased from 3.27 Å to 0.77 Å by 2.5 Å during the CA treatment while that of the Al-OH_2 layer increased from 2.26 to 5.63 Å by 3.37 Å. Assuming that a part of the Al-oxide layer turned to the Al-OH_2 layer, the turning rate might be estimated to be in the range of 0.25–0.34 Å/min at a temperature of 50 °C.

Fig. 5 represents the XPS C1s spectra obtained before (Pristine) and after (CA) treatment with 0.1 wt% CA solution for 10 min at a temperature of 50 °C, demonstrating that the treatment process effectively reduces surface contamination on Al electrodes and induces the formation of an ultrathin surface layer that enhances water molecule adsorption. In Fig. 5(a), curve-fitting analysis of the spectrum measured

Table 2
Calculated thickness of the composite layer formed on aluminum lines before and after citric acid treatment (unit: Å).

	Layer thickness (Å)	
	Pristine	CA
Al-OH_2	2.26	5.63
Al-oxide	3.27	0.77

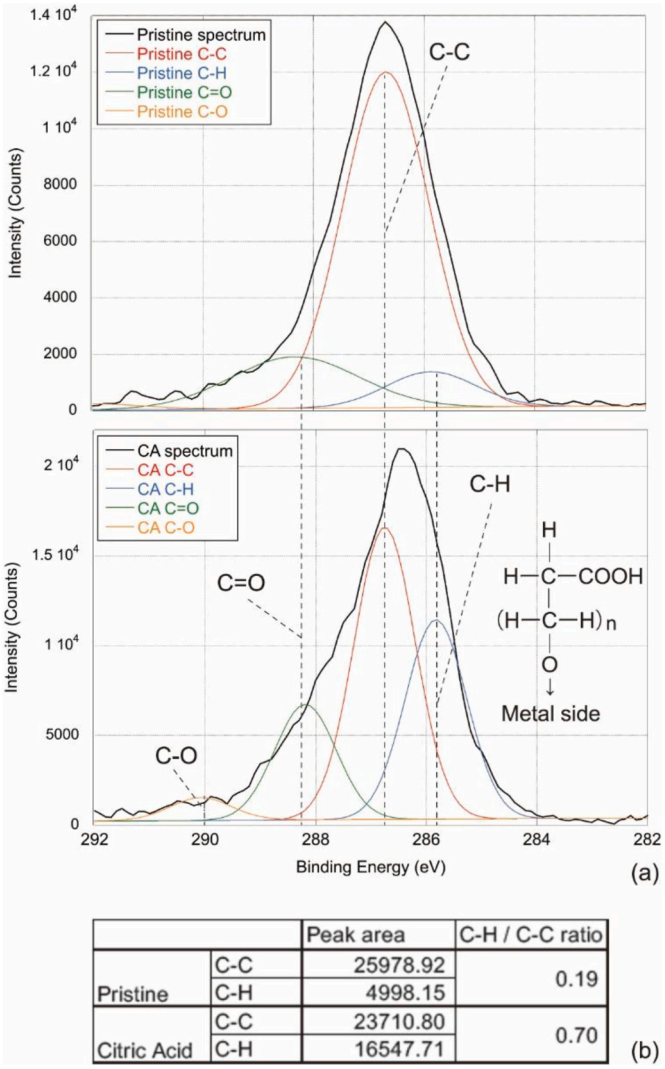

		Peak area	C-H / C-C ratio
Pristine	C-C	25978.92	0.19
	C-H	4998.15	
Citric Acid	C-C	23710.80	0.70
	C-H	16547.71	

(b)

Fig. 5. XPS analysis results showing: (a) the C1s spectra before and after treatment with 0.1 wt% CA solution for 10 min at 50 °C, and (b) the change in the C-H atomic concentration ratio relative to C-C caused by the treatment. An inset schematic in (a) illustrates a possible chemical structure of the surface layer.

at a detection angle of 30° reveals four Gaussian peaks corresponding to C–C, C–H, C=O, and C–O functional groups. These components are presumed to result from reactions between Al or native Al oxide and aqueous CA, as schematically illustrated in the figure inset. Although similar peaks may be present prior to the CA treatment due to residual organic contaminants, the C–C peak was assumed to exhibit the highest atomic concentration under both conditions. Peak fitting was therefore conducted using fixed energy differences relative to the C–C peak [32]. Notably, CA treatment resulted in increased peak intensities of C–H, C=O (carboxyl group), and C–O (hydroxyl group) relative to C–C. As shown in Fig. 5(b), the area ratio of the C–H peak increased markedly from 0.19 before treatment to 0.70 after treatment, providing further evidence for the formation of a chemically modified surface layer. The stretching of the main chain leads to an increase of hydrophilic functional groups on the side chains, supporting the experimental observation of enhanced water adsorption on the treated surface.

Fig. 6 shows the ATR-FTIR spectra of the test chip before (Pristine) and after (CA) treatment with 0.1 wt% CA solution for 10 min at a temperature of 50 °C. The pristine sample showed numerous absorption peaks at 740, 814, 918, and 1026 cm^{-1}, which could be attributed to the stretching vibrations of the mixed oxide and hydroxide layers on the

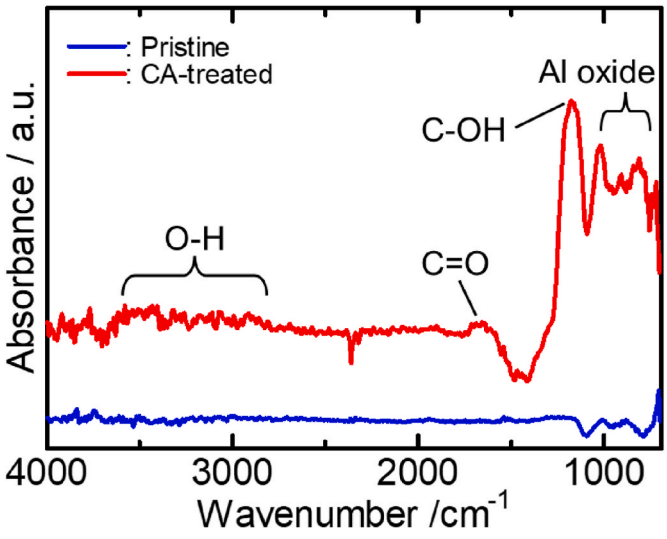

Fig. 6. ATR–FTIR spectra of the chip surface before and after 0.1 wt% citric acid treatment at 50 °C represented by Pristine and CA-treated, respectively.

aluminum surface [33,34]. The peak at 1182 cm^{-1} can be attributed to the stretching vibration of the C-OH group that exists naturally on the pristine chip under atmospheric conditions. The additional peak at 1690 cm^{-1} could be attributed to the stretching vibration from the C=O group. Notably, the pristine chip surface might be covered with a carboxylic resin compound and hydrated Al oxide during the fabrication process. The C-related peaks can be attributed to the remaining of this resin. The FTIR absorption spectra of the CA-treated surface demonstrated no evident peaks correlated to the oxide layer for Al and to the C-related compounds. These findings confirm the successful removal of the inert contamination layer by removing the surface of the oxide layer from the Al lines on the chip.

Fig. 7 shows the optical and scanning electron microscopic images of the test chip before (Pristine) and after (CA) treatment with 0.1 wt% CA solution for 10 min at 50 °C. These images reveal no significant damage to the morphology, that is, the pattern resolution, between Pristine and CA. Moreover, the contrast of the aluminum line in the second-electron SEM image became stronger after the CA treatment. Under the same observation SEM conditions, i.e., the same operator and the same acceleration voltage of the electron beam, a difference in the contrast on the Al lines was found in some locations before and after the CA treatment, whereas the Au lines showed largely the same contrast. Therefore, these results imply that the electrical conductivity around the surface of the Al line might have increased owing to oxide removal.

Fig. 8(a) shows the galvanic current measured from the test chip during the treatment in 0.1 wt% CA aqueous solution at 50 °C. The galvanic current increased sharply and linearly from 1000 to 9000 pA, indicating a decrease in the electrical resistance between the Al and Au lines. The slope in the linear region of the current with time was calculated as $\Delta = dI/dt$. Similarly, the slope during the surface treatment at temperatures of 25 and 75 °C was calculated, and the estimated slope values (current per unit time) in the logarithmic scale were plotted as a function of the reciprocal of the treatment temperature in Kelvin. Similar results were obtained using different chips. As shown in Fig. 8 (b), a largely linear relationship, such as the Arrhenius plot, can be observed between them, suggesting the involvement of a chemical reaction in the surface treatment process of the test chip by CA and that it is governed by kinetics.

From these results, the following model of the phenomenon observed during the surface treatment of aluminum on the chip with CA was proposed: a) decrease in the thickness of the native oxide layer and b) increase in the water adsorption ability, as illustrated in Fig. 9. With regard to a), it can be said that dielectric breakdown is more likely to

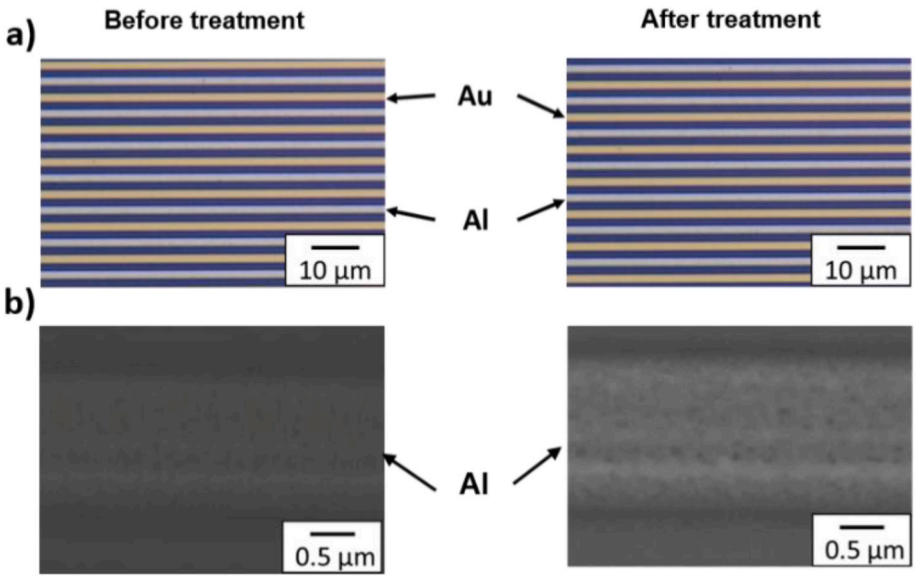

Fig. 7. Optical microscopic images a) and SEM images b) of chip surface before and after 0.1 wt% citric acid treatment at 50 °C.

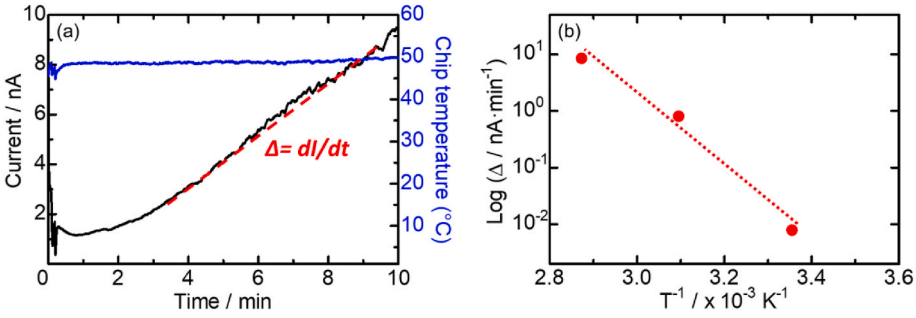

Fig. 8. Temporal changes in the galvanic current and temperature of the test chip during its surface treatment with 0.1 wt% CA solution at 50 °C (a) and relationship between the slope in the current versus time and inverse of the temperature (b).

occur on the CA-treated Al surfaces than on the pristine samples. This may have resulted in the prompt generation of a galvanic current between the Al and Au lines. Regarding factor b), it is postulated that the CA solution forms a new hydrate and/or carboxylic thin surface layer on the deoxidized Al surface, which has a higher number of hydrophilic functional groups than pristine Al. This mechanism is supported by a previous result in that a Al–citric complex is formed through the surface coordination of citrate anion on aluminum hydroxide [21,22].

3.2. Enhancement in sensor response to moisture

Fig. 10(a) shows the variation in the response current of the chip treated with 0.1 wt% CA solution at different times with the stepwise increase in the relative humidity (RH) on its surface. In the region below 100 %RH, a relatively low current was observed because of the agglomeration of adsorbed water molecules between the metal lines on the chip [6]. This study found that the current increased with the treatment time and temperature when compared at the same humidity. When the relative humidity on the chip surface exceeded 100 %RH, the response current showed a rapid increase before and after the CA treatment, regardless of the conditions. This rapid increase in the response current is due to the detection of water droplets generated by dew condensation and their growth [35]. Fig. 10(b) shows the mean value of the response current measured at 100 %RH, plotted as a function of the accumulation time of the surface treatment with CA and superimposed at different treatment temperatures. The response current from the chip treated at 75 °C was 1000 times higher than that in the non-treated case. With an increase in the treatment temperature, the required accumulation time decreased. In other words, the chip surface can be treated in a shorter time at higher temperatures. This is revealed in the fact the steady current response could be achieved within 2–5 min of the treatment at 75 °C.

4. Conclusions

A simple surface treatment method was employed to alleviate the formation of an oxide layer that is inevitably formed on the surface of Al arrays during atmospheric heat treatment. Along with carbon contamination, the oxide layer affects the applicability of Al as a conductive material in the semiconductor and electronics fields. We treated Al arrays on our sensor chip with a 0.1 wt% aqueous solution of citric acid (CA) while investigating the dynamic interaction mechanism and improvement in its characteristics as a moisture sensor. Post-treatment results showed the removal of carbon-based contamination and oxides from the sensor chip. Most of the aluminum oxide on the aluminum lines became hydrophilic owing to the modification with organic molecules derived from CA. The turning rate of the oxide was estimated to be approximately 0.3 Å/min at 50 °C. The sensor response to humid gas dramatically improved by more than 1000 in a shortened time of 2–3 min, presumably given the decreased electrical resistance between the Au and Al arrays. Thus, a stable moisture sensor with minimized surface resistivity could be successfully obtained for a more accurate detection

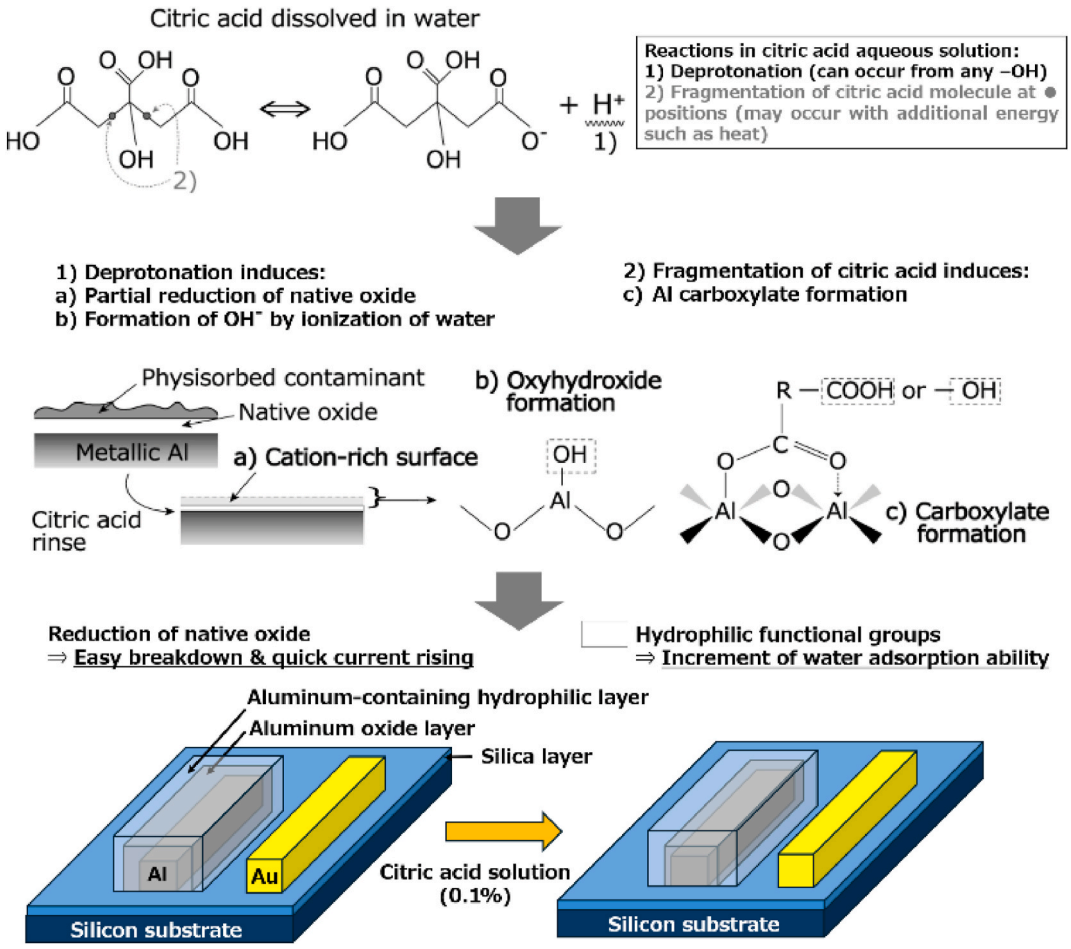

Fig. 9. Proposed schematic of citric acid interaction with Al and Au arrays on chip.

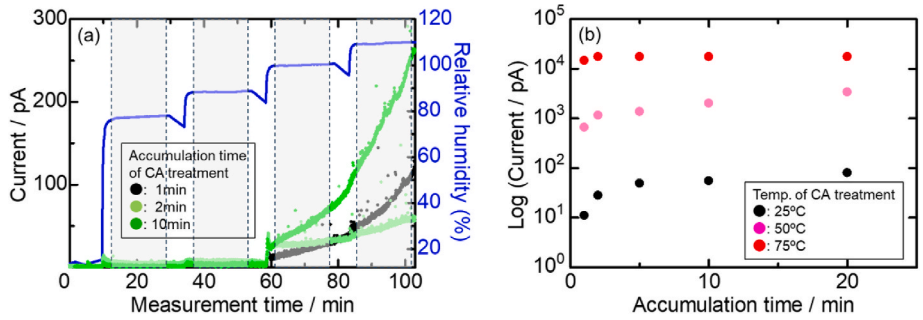

Fig. 10. Current response from chip treated with 0.1 wt% citric acid (CA) solution for accumulation times of 1, 2, and 10 min at 25 °C as a function of the relative humidity (a). Comparison of the response current measured at a relative humidity of 100 % with chips treated at different accumulation times and temperatures of 25, 50, and 75 °C (b).

of the relative humidity along with a longer lifetime.

CRediT authorship contribution statement

Moataz Mekawy: Writing – original draft, Formal analysis, Data curation. **Kazuya Iida:** Investigation, Data curation. **Akitsu Shigetou:** Writing – review & editing, Validation, Resources, Methodology, Investigation, Formal analysis, Data curation, Conceptualization. **Jin Kawakita:** Writing – review & editing, Validation, Supervision, Resources, Project administration, Methodology, Funding acquisition, Data curation, Conceptualization.

Declaration of competing interest

The authors declare the following financial interests/personal relationships which may be considered as potential competing interests: The sensor chips and the measurement devices in this research included those provided free of charge by Aquze, co. Ltd. One of the authors, J. Kawakita is holding a post concurrently on Aquze.

Acknowledgment

This research was supported by the Startup Supporting Program (funding agency: Bio-Oriented Technology Research Advancement

Institution (Brain)) under Grant Number JPJ010717. Authors acknowledge Ms. Venkategowda Mala for her contribution in the experimental work of the electrical measurement.

Appendix

The sensor chips and measurement devices used in this study included those provided free of charge by Aquze Co., Ltd. One of the authors, J. Kawakita, held a post concurrently with Aquze.

Data availability

Data will be made available on request.

References

[1] Coker, E.N., Donaldson, B., Gill, W., Yilmaz, N., Vigil, F.M., 2023. The isothermal oxidation of high-purity aluminum at high temperature. Appl. Sci. 13, 229. https://doi.org/10.3390/app13010229.
[2] Trunov, M.A., Schoenitz, M., Dreizin, E.L., 2006. Effect of polymorphic phase transformations in alumina layer on ignition of aluminum particles. Combust. Theor. Model. 10, 603–623. https://doi.org/10.1080/13647830600578506.
[3] Kolarik, V., del Mar Juez-Lorenzo, M., Fietzek, H., 2011. Oxidation of micro-sized spherical aluminum particles. Mater. Sci. Forum 696, 290–295. https://doi.org/10.4028/www.scientific.net/MSF.696.290.
[4] Szklarska-Smialowska, Z., 1999. Pitting corrosion of aluminum. Corros. Sci. 41, 1743. https://doi.org/10.1016/S0010-938X(99)00012-8.
[5] Kawakita, J., Chikyow, T., 2017. Detection of micro/nano droplet by galvanic-coupled arrays. ECS Trans. 75, 51–59. https://doi.org/10.1149/07529.0051ecst.
[6] Mekawy, M., Terada, E., Kawakita, J., 2022. Quantitative correlation between adsorbed and condensed water mass with response galvanic current detected at the micron gap of galvanic-coupled arrays. Chemosensors 10, 300. https://doi.org/10.3390/chemosensors10080300.
[7] Mekawy, M., Kazuya, I., Satoh, N., Sakamoto, Y., Kawakita, J., 2024. Refinement of thermal conduction-based dew condensation detection on target solid surface by galvanic arrays sensor chip, nanoscale and microscale thermophys. Engineer 28, 46–58. https://doi.org/10.1080/15567265.2023.2285745.
[8] Sheasby, P.G., Pinner, R., 2001. The Surface Treatment and Finishing of Aluminum and its Alloys, sixth ed. Finishing Publications Ltd. and ASM International.
[9] Deng, J., Zhao, G., Lei, J., Zhong, L., Lei, Z., 2022. Research progress and challenges inlaser-controlled cleaning of aluminum alloy surfaces. Materials 15, 5469. https://doi.org/10.3390/ma15165469.
[10] Hara, K., 2018. Pre-treatment in the surface treatment of aluminum. J. Surf. Finish. Soc. Jpn. 69, 380–383. https://doi.org/10.4139/sfj.69.380.
[11] Poznyak, A., Pligovka, A., Turavets, U., Norek, M., 2020. On-Aluminum and barrier anodic oxide: meeting the challenges of chemical dissolution rate in various acids and solutions. Coatings 10, 875. https://doi.org/10.3390/coatings10090875.
[12] Rahide, F., Palanisamy, K., Flowers, J.K., Hao, J., Stein, H.S., Kranz, C., Ehrenberg, H., Dsoke, Sonia, 2024. Modification of Al surface via acidic treatment and its impact on plating and stripping. ChemSusChem 17, e202301142. https://doi.org/10.1002/cssc.202301142.
[13] Wongchaiya, P., Ngan Nguyen, T.K., Sujaridworakun, P., Larpkiattaworn, S., Suzuki, T.S., Uchikoshi, T., 2024. Fabrication of g-C_3N_4 films with enhanced mechanical and charge transfer properties by electrophoretic deposition and subsequent citric acid modification. Adv. Powder Technol. 35, 104460. https://doi.org/10.1016/j.apt.2024.104460.
[14] Salihu, R., Razak, S.I.A., Zawawi, N.A., Kadir, M.R.A., Ismail, N.I., Jusoh, N., Mohamad, M.R., Nayan, N.H.M., 2021. Citric acid: a green cross-linker of biomaterials for biomedical applications. Eur. Polym. J. 146, 110271. https://doi.org/10.1016/j.eurpolymj.2021.110271.
[15] Cui, X., Ozaki, A., Asoh, T.A., Uyama, H., 2020. Cellulose modified by citric acid reinforced poly (lactic acid) resin as fillers. Polym. Degrad. Stabil. 175, 109118. https://doi.org/10.1016/j.polymdegradstab.2020.109118.
[16] Reddy, N., Yang, Y., 2010. Citric acid cross-linking of starch films. Food Chem. 118, 702–711. https://doi.org/10.1016/j.foodchem.2009.05.050.
[17] Lee, S.H., Tahir, P.M., Lum, W.C., Tan, L.P., Bawon, P., Park, B.-D., Edrus, S.S.O.A., Abdullah, U.H., 2020. A review on citric acid as green modifying agent and binder for wood. Polymer 12, 1692. https://doi.org/10.3390/polym12081692.
[18] Ciriminna, R., Meneguzzo, F., Delisi, R., Pagliaro, M., 2017. Citric acid: emerging applications of key biotechnology industrial product. Chem. Cent. J. 11, 22. https://doi.org/10.1186/s13065-017-0251-y.
[19] Mikelashvili, V., Kekutia, S., Markhulia, J., Saneblidze, L., Maisuradze, N., Kriechbaum, M., Almásy, L., 2023. Synthesis and characterization of citric acid-modified iron oxide nanoparticles prepared with electrohydraulic discharge treatment. Materials 16, 746. https://doi.org/10.3390/ma16020746.
[20] Shinohara, S., Eom, N., Teh, E.-J., Tamada, K., Parsons, D., Craig, V.S.J., 2018. The role of citric acid in the stabilization of nanoparticles and colloidal particles in the environment: measurement of surface forces between hafnium oxide surfaces in the presence of citric acid. Langmuir 34, 2595–2605. https://doi.org/10.1021/acs.langmuir.7b03116.
[21] Hidber, P.C., Graule, T.J., Gauckler, L.J., 1996. Citric acid- A dispersant for aqueous alumina suspensions. J. Am. Ceram. Soc. 79, 1857–1867. https://doi.org/10.1111/j.1151-2916.1996.tb08006.x.
[22] Seruga, M., Hasenay, D., 2001. Electrochemical and surface properties of aluminum in citric acid solutions. J. Appl. Electrochem. 31, 961–967. https://doi.org/10.1023/A:1017556323508.
[23] Seri, O., Ssakai, M., 2004. Effect of citric acid on corrosion behavior of 1100 aluminum. J. Jap. Inst. Light Met. 54, 19–24. https://doi.org/10.2464/jilm.54.19.
[24] Shrestha, R.G., Kawakita, J., 2023. Continuously activated function of aluminum in galvanic micro arrays in contact with water. J. Electrochem. Soc. 170, 087505. https://doi.org/10.1149/1945-7111/aceab3.
[25] Strohmeier, B.R., 1990. An ESCA method for determining the oxide thickness on aluminum alloys. Surf. Interface Anal. 15, 51–56. https://doi.org/10.1002/sia.740150109.
[26] Moulder, J.F., Stickle, W.F., Sobol, P.E., Bomben, K.D., 1992. Handbook of X-ray Photoelectron Spectroscopy. Perkin-Elmer Corporation, Eden Prairie, Minnesota, USA. ISBN: 0-9627026-2-5.
[27] Olefjord, I., Mathieu, H.J., Marcus, P., 1990. Intercomparison of surface analysis of thin aluminium oxide films. Surf. Interface Anal. 15, 681–692. https://doi.org/10.1002/sia.740151108.
[28] Lindsay, J.R., Rose, H.J., Swartz, W.E., Watts, P.H., Rayburn, K.A., 1973. X-ray photoelectron spectra of aluminum oxides: structural effects on the “chemical shift”. Appl. Spectrosc. 27, 1–5. https://doi.org/10.1366/000370273774333876.
[29] Klein, C., Hercules, D.M., 1983. Surface characterization of model Urushibara catalysts. J. Catal. 82, 424–441. https://doi.org/10.1016/0021-9517(83)90209-9.
[30] Yang, H.W., Kao, C.R., Shigetou, A., 2017. Fast atom beam- and vacuum-ultraviolet-activated sites for low-temperature hybrid integration. Langmuir 33, 8413–8419. https://doi.org/10.1021/acs.langmuir.7b02010.
[31] NIST electron inelastic-mean-free-path database: Version 1.2. https://doi.org/10.18434/T48C78.
[32] Beamson, G., Briggs, D., 1993. High resolution XPS of organic polymers: the scienta ESCA300 database. J. Chem. Educ. 70 (5), A25. https://doi.org/10.1021/ed070pA25.
[33] Atrak, K., Ramazani, A., Fardood, S.T., 2018. Green synthesis of amorphous and gamma aluminum oxide nanoparticles by tragacanth gel and comparison of their photocatalytic activity for the degradation of organic dyes. J. Mater. Sci. Mater. Electron. 29, 8347–8353. https://doi.org/10.1007/s10854-018-8845-2.
[34] El-Khawaga, A.M., Farrag, A.A., Elsayed, M.A., El-Sayyad, G.S., El-Batal, A.I., 2022. Promising antimicrobial and azo dye removal activities of citric acid-functionalized magnesium ferrite nanoparticles. J. Cluster Sci. 33, 197–213. https://doi.org/10.1007/s10876-020-01944-y.
[35] Terada, E., Mekawy, M., Sakamoto, Y., Kawakita, J., 2021. Relation between water status on micro/nano gap between galvanic arrays and flowing current around 100% in relative humidity. J. Electrochem. Soc. 168, 047512. https://doi.org/10.1149/1945-7111/abf7e6.